Intermittent fasting promotes adipocyte mitochondrial fusion through Sirt3-mediated deacetylation of Mdh2

Yizhou Li, Juntong Liang, Xin Tian, Qi Chen, Longbo Zhu, Han Wang, Zunhai Liu, Xulei Dai, Chenqi Bian and Chao Sun*

College of Animal Science and Technology, Northwest A&F University, Yangling, Shaanxi 712100, People's Republic of China

Abstract

Fat deposition and lipid metabolism are closely related to the morphology, structure and function of mitochondria. The morphology of mitochondria between fusion and fission processes is mainly regulated by protein posttranslational modification. Intermittent fasting (IF) promotes high expression of Sirtuin 3 (Sirt3) and induces mitochondrial fusion in high-fat diet (HFD)-fed mice. However, the mechanism by which Sirt3 participates in mitochondrial protein acetylation during IF to regulate mitochondrial fusion and fission dynamics remains unclear. This article demonstrates that IF promotes mitochondrial fusion and improves mitochondrial function in HFD mouse inguinal white adipose tissue. Proteomic sequencing revealed that IF increased protein deacetylation levels in HFD mice and significantly increased Sirt3 mRNA and protein expression. After transfecting with Sirt3 overexpression or interference vectors into adipocytes, we found that Sirt3 promoted adipocyte mitochondrial fusion and improved mitochondrial function. Furthermore, Sirt3 regulates the JNK-FIS1 pathway by deacetylating malate dehydrogenase 2 (MDH2) to promote mitochondrial fusion. In summary, our study indicates that IF promotes mitochondrial fusion and improves mitochondrial function by upregulating the high expression of Sirt3 in HFD mice, promoting deacetylation of MDH2 and inhibiting the JNK-FIS1 pathway. This research provides theoretical support for studies related to energy limitation and animal lipid metabolism.

Key words: Intermittent fasting: Sirt3: Deacetylation: Mitochondrial dynamics: Mitochondrial function

Mitochondria act as organelles that regulate a series of functions, such as lipid metabolism, energy production, calcium homeostasis and cell death. Therefore, regulating mitochondrial morphology and energy production plays an important role in maintaining cell health[1]. Mitochondrial fusion, fission and biogenesis determine the shape, quality and quantity of mitochondria, and also sense metabolic cues or respond to energy changes to maintain the function of mitochondria[2]. Mitochondrial morphology is regulated by the balance between fusion and fission, and cells adjust mitochondrial morphology to coordinate the relationship between energy requirements and resource availability. Mitochondrial fusion leads to morphological extension, which increases the efficiency of ATP production, reduces the production of reactive oxygen species (ROS), exchanges mitochondrial DNA (mtDNA) and other matrix components between mitochondria and promotes oxidative phosphorylation[3]. According to reports[4], two GTPase mitochondrial fusion proteins mitofusin 1 and 2 (MFN1/2) mediate mitochondrial outer membrane fusion, and optic atrophy protein 1 (OPA1) mediates mitochondrial inner membrane fusion. Mitochondrial fission is related to mitochondrial uncoupling and allows dysfunctional mitochondria to separate into mitochondrial targets[5]. In mammals, dynamin-related protein 1 (DRP1) is recruited to the mitochondrial outer membrane and combines with receptor proteins at the mitochondrial outer membrane, including mitochondrial fission protein 1 (FIS1), mitochondrial fission factor (MFF) and mitochondrial dynamics proteins of 49 and 51 kDa (MID49 and MID51). Eventually, these proteins oligomerise to form ring structures that separate mitochondria via constriction[6]. The integration of mitochondrial dynamics and the state of cell bioenergy can maintain the stability of mitochondrial quality and respond to bioenergy stress[7]. Research on mitochondrial dynamics shows that there is a strong connection between energy requirements/supply and mitochondrial morphology. The nutrient-rich environment separates mitochondria, while a starvation environment promotes mitochondrial fusion[8]. Therefore, bioenergetic adaptation may be associated with the remodelling of mitochondrial morphology.

Currently, intermittent fasting (IF) has been used as an effective method to control weight and improve metabolic health[9].

IF is mainly divided into intermittent energy restriction and time-restricted feeding. Growing evidence demonstrates the advantage of intermittent energy restriction in improving glucose and lipid homeostasis in short to medium term and preventing high-fat diet (HFD)-induced obesity and insulin resistance[10,11]. Moreover, IF requires dynamic network remodelling through fusion and fission to maintain mitochondrial homeostasis[12]. The regulation of mitochondrial morphology is essential for cell energy homeostasis. However, whether the preventive effect of IF on diet-induced obese mice is related to the mitochondrial morphology within adipose tissue remains unknown.

Sirtuin 3 (Sirt3) regulates metabolism and protein acetylation during intermittent food deprivation or fasting[13]. Studies have shown that Sirt3 expression increases significantly during fasting, which reduces the degree of acetylation of fatty acid β-oxidation-related enzymes[14]. Sirt3-mediated trifunctional enzyme subunit α deacetylation directly promotes fatty acid β-oxidation and the content of trichloroacetic acid, decreases the lipid signalling which leads to insulin secretion and regulates the production of ATP[14,15]. Knockdown of Sirt3 fails to cause continuous cytoplasmic ATP production, increases acetylation of mitochondrial enzymes that participate in fatty acid β-oxidation, the tricarboxylic acid cycle (TCA) and the electron transport chain, and weakens calcium signal transduction[16,17]. Therefore, lysine acetylation is closely related to the metabolic state. In recent years, studies have demonstrated that a large number of proteins located in the mitochondria (the energy centre of cells) can be modified by lysine acetylation[18]. This modification mainly relies on the Sirtuin family of nicotinamide adenine dinucleotide (NAD)+-dependent deacetylases[19]. In addition, OPA1 is deacetylated and activated by Sirt3 to exert its mitochondrial fusion function. When Sirt3 is absent, OPA1-mediated mitochondrial fusion function is inhibited[20]. This connects protein acetylation modifications with energy metabolism controlled by mitochondrial dynamics.

Recent work has shown the importance of reversible protein acetylation, such as changing the activity of class I HDAC and/ or Sirtuin to maintain mitochondrial biological function and energy metabolism during normal heart and ischaemia–reperfusion injury[21,22]. It is important to combine metabolomics and epigenomics techniques to reveal the mechanism that controls the dynamic changes in mitochondrial dynamics caused by the epigenetic modification of energy limitations caused by mitochondrial proteins. Changes in energy and nutrition lead to significant fluctuations in mitochondrial proteins and control the fate of mitochondria through post-translational modification. We deeply investigated the regulation of mitochondrial morphology through epigenetics and the regulation of cellular and the global energy metabolism. Our research provides several new ideas for the treatment and improvement of metabolic diseases, such as obesity, and for the maintenance of global energy metabolism in mammals.

Methods

Animal experiment

All experimental protocols were approved by the guidelines and regulations approved by the Animal ethics committee of Northwest A&F University (DK2022063). C57BL/6J male mice were purchased from the Laboratory animal centre of the fourth Military Medical University. ob/ob mice were purchased from VIEWSOILD. Initially, twenty-four 6-week-old C57BL/6J male mice were randomly divided into four groups (*n* 6 each). Mice were housed on a 12-h light/dark cycle and had free access to food and water. The researchers recorded the changes in body weight and food intake of the mice every 2 d. Two groups of mice were fed the standard chow diet (Chow, fat provided 10 % of total energy, Trophic Animal Feed High-tech Co., Ltd), and the other two groups were fed the HFD (fat provided 60 % of the total energy, Trophic Animal Feed High-tech Co., Ltd). In addition, twelve ob/ob mice were randomly divided into two groups (*n* 6 each) and housed under the same conditions, with all ob/ob mice fed the HFD and fed an *ad libitum* diet for 12 weeks. In the second phase, six groups of mice were treated with IF, which divided the mice into six groups, wild-type (WT) (*n* 6), WT-IF (*n* 6), HFD (*n* 6), HFD-IF (*n* 6), ob/ob (*n* 6) and ob/ob-IF (*n* 6). The WT, HFD and ob/ob groups were fed under the same conditions as the *ad libitum*, WT-IF, HFD-IF and ob/ob-IF mice, which were treated with IF. The IF group was fed *ad libitum* for 8 h (23:00–7:00), and fasting was administered for the remaining 16 h (7:00–23:00). The second phase lasted for 4 weeks. Finally, tissue was collected after overnight fasting. Blood samples were collected from all six groups of mice by orbital blood sampling after overnight fasting, and the serum was collected by centrifugation and stored at −80°C for testing. Serum samples were tested to detect multiple biochemical parameters using serum biochemical indicator kits, including total cholesterol (TC, Jiancheng), total TAG (Jiancheng), HDL (Jiancheng) and LDL (Jiancheng).

Cell culture

Overexpression plasmid vectors of sirt3 (pc-Sirt3) were constructed in our lab (F: 5′-CCCAAGCTTATGGCGCTTGACC CTCTAGG-3′, R: 5′-TGCTCTAGATTATCTGTCCTGTCCATCCA GC-3′, Hind III: AAGCTT, Xba I: TCTAGA), and the interference vectors of Sirt3 were constructed by TSINGKE.

The frozen 3T3-L1 adipose precursor cells (Shanghai Bioleaf Biotech Co) were resuscitated, passaged and plated. Cells were cultured in DMEM containing 10 % foetal bovine serum and placed in a humidified incubator at 37°C and 5 % CO_2. Transfection was performed when the cell density reached approximately 75 %. Taking a six-well plate as an example, approximately 6 h before transfection, the medium was changed to serum-free medium without penicillin–streptomycin solution. 2 μg of recombinant plasmid and 2 μl of transfection reagent were added to the serum-free medium, vortexed to mix and incubated for 20 min. The mixed solution was added to a petri dish and placed in an incubator for 6 h and was then replaced with a normal culture medium. After 48 h, induction solution I (IBMX: 0·5 mmol/l, Dex: 1 mmol/l, insulin: 10 ug/ml) was added for 2 d, and then induction solution II (insulin: 10 ug/ml) was switched for 8 d. After 8 d, the cells were collected for further processing. For drug treatment, JNK inhibitor SP600125 (SP)

and activator Anisomycin (Ani) were purchased from MedChemExpress. In accordance with previous studies[23,24], cells were incubated with 10 μM SP600125 or 1 μg/ml anisomycin for 30 min.

Transmission electron microscopy and mitochondrial analysis

Mouse inguinal white adipose tissue (iWAT) was collected immediately after execution, quickly cut into 1 mm × 1 mm × 1 mm pieces, placed in 2·5 % glutaraldehyde (0·1 M, pH 7·2–7·4) for 24 h, and rinsed three times in PBS buffer (pH 7·2, 0·1 mol/l) for 15 min each. Tissue was dehydrated using an ethanol gradient (30 %, 50 %, 70 %, 80 %, 90 % and 100 %) twice for 10 min each. Next, resin infiltration was performed with 25 % embedding agent for 2 h, 50 % embedding agent for 8 h, 75 % embedding agent for 12 h and pure embedding agent twice, each time at room temperature for 24 h. Subsequent embedding was performed using embedding mould and cured in an oven at 55°C for 48 h. After curing, the sections were sectioned using an ultrathin sectioning machine. Staining was conducted using 2 % UO2 acetate for 30 min and lead citrate for 10 min. After staining, sections were observed under transmission electron microscopy (TEM).

For mitochondrial aspect ratio analysis, according to previous studies[25], each individual mitochondrial in the electron microscopy images was manually outlined using ImageJ software (n 8 each group). Mitochondrial marker consistency checks were performed twice on all samples. We used the mitochondrial aspect ratio (AR = long axis/short axis) as a measure of mitochondrial shape.

Mitochondrial isolation and Janus Green B staining

The mitochondrial extraction kit was purchased from Solarbio. Fresh mouse iWAT (100–200 mg) was rinsed with PBS, cut into pieces and placed in a small volume glass homogenizer. Next, 1·0 ml of ice precooled lysis buffer was added, and the tissue was homogenised thirty times in an ice bath at 0°C. The homogenised tissue was transferred to a centrifuge tube and centrifuged at 1000 × g for 5 min at 4°C. The supernatant was removed, transferred to a new tube and centrifuged at 1000 × g for 5 min at 4°C. The supernatant was removed, transferred to a new tube and centrifuged at 12 000 × g for 10 min at 4°C. Next, 0·5 ml of wash buffer was added to the sediment, and the mitochondrial sediment was resuspended at 1000 × g for 5 min at 4°C. The supernatant was transferred to a new tube and centrifuged again at 4°C, 12 000 × g for 10 min. The supernatant was discarded, and the mitochondrial precipitate was resuspended in 50 μl of Store buffer to obtain complete and purified mitochondria for immediate use for experiments or storage at −70°C.

The freshly extracted mitochondria were mixed with Janus Green B staining solution (0·05 %) (Solarbio) for 3 min and observed under a fluorescence microscope.

JC-1 staining

The JC-1 staining kit was purchased from UE. It is a fluorescent probe widely used to detect mitochondrial membrane potential.

Mitochondria were extracted from 100 to 200 mg mouse iWAT, and the mitochondrial precipitate from the last step was retained (without Store Buffer) and added directly into 0·5 ml of JC-1 working solution (10 μl of 100 × JC-1 staining solution was added to 890 μl of sterilised diH$_2$O, mixed well followed by the addition of 100 μl of 10 × Assay Buffer, that was then vortexed to fully mix). Mitochondria were resuspended, incubated at 37°C for 15 min and centrifuged at 1000 × g for 5 min at room temperature. The staining solution was removed, and the precipitates were washed twice with PBS buffer. Finally, the precipitate was resuspended in 0·5 ml PBS and observed under a fluorescence microscope. The mitochondria fluoresced red at 590 nm and green at 530 nm.

NAD+ detection

NAD+ content assay kit was purchased from Nanjing Jiancheng Bioengineering Institute. Mouse iWAT (0·1 g) or 5 × 10^6 cells were added to 1 ml of acidic extract, ground in an ice bath, boiled for 5 min, cooled on ice and centrifuged at 10 000 × g for 10 min at 4°C. The supernatant was mixed with an equal volume of alkaline extract and centrifuged at 10 000 × g for 10 min at 4°C. After tissue samples fully reacted with the test reagents in the kit according to the instructions, the absorbance was measured at 570 nm with a 1-cm optical diameter cuvette. The sample reaction product was recorded as A1 and the control product was recorded as A0. NAD+ content: NAD+ (μmol/g tissue or nmol/10^4 cells) = (A1-A0–0·099) x 72·2 ÷ 0·1 × 1000.

ATP detection

The ATP content assay kit was purchased from Nanjing Jiancheng Bioengineering Institute. For mouse iWAT samples, 0·1 g iWAT was accurately weighed, 900 μl of preboiled double-distilled water was added to prepare a 10 % homogenate that was placed in boiling water for 10 min, mixed and extracted for 1 min and then centrifuged at 3500 rpm for 10 min and the supernatant was taken for measurement. Samples and reagents in the kit were mixed and reacted thoroughly according to the instructions. The absorbance of the products was measured at 636 nm using a 0·5-cm optical diameter cuvette. The absorbance of the control group was recorded as A0 and that of the sample was recorded as A1. The absorbance of the blank control was recorded as A2 and that of the standard was recorded as A3. Tissue ATP concentration: ATP (nmol/mg protein) = (A1-A0)/(A3-A2) × Cstandard (1 × 103 nmol/ml) ÷ Csample (protein concentration). The protein concentration of the product supernatant was determined using the BCA protein concentration kit (Solarbio).

For cell samples, 10^6 cells were collected and 300–500 μl of preboiled double-distilled water was added and placed in boiling water to homogenise and break up. To prepare for the assay, the cell suspension was heated in boiling water for 10 min, mixed and extracted for 1 min. The subsequent assay and calculations were the same as those for the tissue samples.

Measurement of mtDNA copy number

Total DNA was extracted from mouse iWAT or 3T3-L1 adipocytes using the Animal Tissues/Cells Genomic DNA Extraction

Kit (Solarbio). The mtDNA copy number was detected by qPCR with the following reagents: The mitochondrial DNA was represented by the gene primer sequence encoded by 12 s RNA, primer sequence: mtDNA-F: ACCGCGGTCATACGATTAAC, mtDNA-R: CCCAGTTTGGGTCTTAGCTG. The nuclear-encoded Gcg gene was used to represent nuclear DNA as a loading control, primer sequences: nucDNA-F: CAGGGCCATCTCAGAACC, nucDNA-R: GCTATTGGAAAGCCTCTTGC.

Reactive oxygen species fluorescence detection

The ROS detection kit was purchased from UE. DCFH-DA, a fluorescent probe specific for intracellular ROS, can pass freely through the cell membrane into living cells and is hydrolysed by intracellular esterases to form DCFH, which is nonfluorescent and cannot pass through the cell membrane and is then oxidised by intracellular ROS to produce DCF with fluorescence. After cell culture, DCFH-DA was diluted 1:1000 with serum-free medium to a final concentration of 10 µM. The original medium was removed from the plates and an appropriate volume (no less than 1 ml for six-well plates) of DCFH-DA was added and incubated for 30 min at 37°C in a cell culture incubator protected from light. After incubation, the cells were then washed twice with serum-free medium to fully remove any DCFH-DA that had not entered the cells and then placed under a fluorescence microscope for observation.

MitoTracker red

MitoTracker Red CMXRos Kit was purchased from Beyotime. When the cells grew to the desired confluency, the medium was removed, and MitoTracker Red CMXRos staining working solution (100 nM, prewarmed at 37°C) was added. The cells were incubated for 40 min under normal culture conditions. After staining, the cells were washed with medium and replaced with freshly prepared and prewarmed buffer containing 2–4 % formaldehyde for cell fixation. After fixation, the cells were washed, and diluted DAPI was added to stain the nuclei for 1 min. The cells were observed under a fluorescence microscope.

Label-free proteomic analysis of acetylation modification of mouse adipose tissue

The sample was removed from −80°C, 100–200 mg of tissue sample was weighed into a mortar precooled with liquid nitrogen and liquid nitrogen was added to fully grind the tissue to a powder. The samples of each group were added to 4 times the volume of lysis buffer (8 M urea, 1 % protease inhibitor, 3 µM trichostatin A (TSA), 50 mM nicotinamide (NAM) and 2 mM EDTA) and lysed ultrasonication. The samples were centrifuged at $12\,000 \times g$ for 10 min at 4°C to remove cell debris, the supernatant was transferred to a new centrifuge tube, and a BCA kit was used to determine the protein concentration. The sample was sent to post-translational modification BIO for trypsin digestion, affinity enrichment, LC/MS analysis, database search and bioinformatics analysis.

CRISPR-Cas9

http://crispr.dbcls.jp/ website and Primer Premier 6·0 primer design software were used to design primer sequences

(Target 1-F: TAGAGTCGAAGTAGTGATTGCGTCAGAGCGAAC ACGTTTG, Target 1-R: GCTATTTCTAGCTCTAAAACCAAACGT GTTCGCTCTGACG, Target 2-F: TAGAGTCGAAGTAGTGATT GGGTGGCCACAATGGTAGCGT, Target 2-R: GCTATTTCTAG CTCTAAAACACGCTACCATTGTGGCCACC, 2300-Cas9-F: GTA AAAC-GACGGCCAGTGCC, 2300-Cas9-R: CAATTTGTGAAATA TCCCGGGG). The target sequences were cloned by PCR. Target 1 and Target 2 were ligated to CAS9-IV plasmids. The product of the previous step was used as a template, and 2300-Cas9 was cloned by PCR with the designed primers. After double digestion of plasmid 2300-CAS9 with HindIII and SmaI, the digestion product was ligated to Target 1-iv and Target 2-iv. The products were quickly transformed into competent cells. The recombinant plasmid was identified by colony PCR, the recombinant plasmid was extracted and positive strains were selected and sent to TSINGKE for sequencing.

RNA extraction and real-time PCR

Total RNA of tissues or cells were extracted with TRIpure Reagent kit (Takara). 500 ng of total RNA was reverse transcribed using an M-MLV reverse transcriptase kit (Takara). Primers were synthesised by Invitrogen. Real-time PCR procedures were performed as described previously[26].The levels of mRNA were normalised to *Gapdh*. The expression of genes was analysed by the $2^{-\triangle\triangle Ct}$ method.

Immunoblotting and antibodies

According to our previous studies[26], protein was isolated from tissues or cultured cells. Western blotting was performed as previously described[26]. Protein samples (30 µg) were separated by electrophoresis on 12 % and 5 % SDS-PAGE gels using a slab gel apparatus and transferred to polyvinylidene fluoride (PVDF) membranes (Millipore). Antibodies against OPA1 (ab157457, Abcam), FIS1(ab156865, Abcam), MFF (ab129075, Abcam), SIRT3(ab189860, Abcam), SIRT1 (ab110304, Abcam), Pan-Kac antibody (ab190479, Abcam), β-actin (ab8226, Abcam), GAPDH(AB0037, Abways), ATF2 (CY5037, Abways), TOM20 (CY5527, Abways), JNK (CY5490, Abways), p-JNK (CY5541, Abways) and the secondary antibody (AB0101, Abways) were used. Proteins were visualised using chemiluminescent peroxidase substrate (Millipore), and then the blots were quantified using the ChemiDoc XRS system (Bio-Rad).

Co-immunoprecipitation and acetylation assay

Co-immunoprecipitation Kit was purchased from Themo. Cells were harvested 48 h after transfection, and cell lysis buffer was added. Subsequent steps were performed in strict accordance with the instructions within the kit. Antibodies against MDH2 (ab110317, Abcam) and Pan-Kac (ab190479, Abcam) antibodies were used.

Glucose tolerance test and insulin tolerance test

For the glucose tolerance test, mice were fasted overnight, glucose (1 g/kg) was administered intraperitoneally (i.p.), and blood glucose levels were measured at 0 min, 30 min, 60 min, 90 min and 120 min using a glucometer.
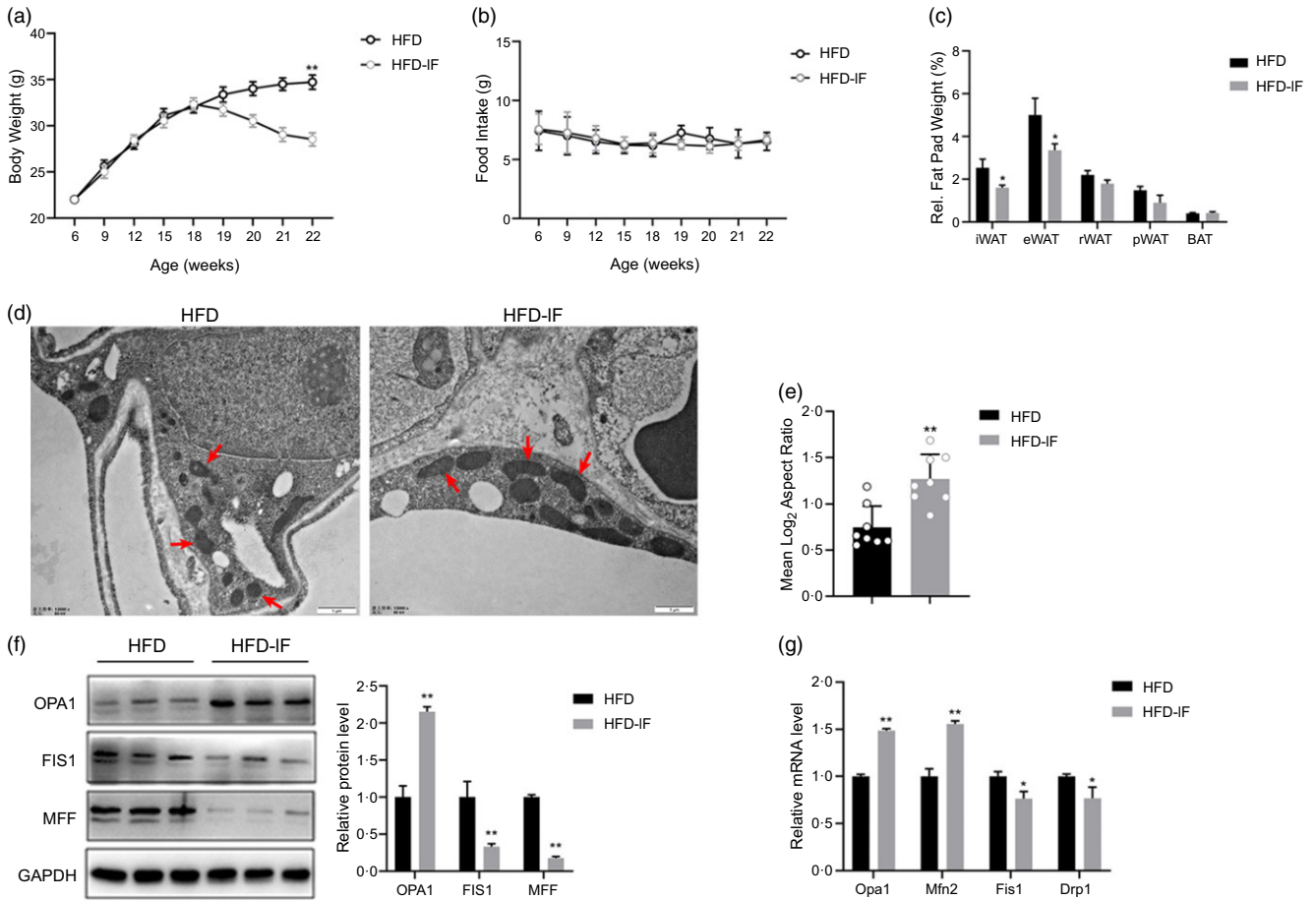
Fig. 1. IF promotes iWAT mitochondrial fusion in HFD mice. (a, b) Body weight (a) and food intake of HFD and HFD–IF mice (HFD n 6, HFD–IF n 6). (c) Weight ratio of adipose tissue to body weight (HFD n 6, HFD–IF n 6). (d) TEM image of HFD (Left) and HFD–IF (Right) mouse iWAT, arrows point to mitochondria. Scale bar, 1 μm. (e) Quantification of mitochondrial aspect ratio, n 8 each group. (f) Western blotting of mitochondrial fusion and division-related protein and its quantification, n 3. (g) RT-qPCR of mitochondrial fusion and division-related gene, n 4. *$P < 0.05$, **$P < 0.01$ compared with control group. Data are mean ± SEM. HFD, high-fat diet; IF, intermittent fasting; TEM, transmission electron microscopy.

For the insulin tolerance test, mice were fasted for 4 h and i.p. injected with insulin (0·75 U/kg), and blood glucose levels were measured at 0 min, 15 min, 30 min, 45 min and 60 min using a glucometer.

Statistical analysis

Statistical analyses were conducted using SPSS (version 19.0). To examine the significant differences between groups, the data were compared using Student's t test, whereas data comparisons across more than two groups were performed using one-way or two-way ANOVA, followed by Bonferroni's post hoc tests. Data were presented as the mean ± SEM. $P < 0.05$ was considered to be significant, and $P < 0.01$ was considered to be highly significant.

Results

Intermittent fasting improves metabolism and promotes mitochondrial fusion in high-fat diet mice

We fed C57BL/6 WT mice a HFD for 12 weeks and then began IF for 4 weeks. After IF, the weight of the mice was significantly reduced ($P < 0.05$), but there was no significant change in food intake (Fig. 1(a) and (b)). After separating the mouse adipose tissues, the weight of each adipose tissue was measured, and the ratio of adipose tissue to body weight was calculated. The most significant reduction was observed in iWAT ($P < 0.05$) (Fig. 1(c)). Furthermore, the blood serum concentrations of major metabolites in the mice were measured, and IF significantly reduced the levels of TC ($P < 0.05$), TAG ($P < 0.05$) and LDL ($P < 0.01$) and had an upwards trend in HDL ($P = 0.068$) (online Supplementary Fig. S1A). We also found that IF improved glucose tolerance in HFD mice (online Supplementary Fig. S1B). Adipose tissue is a key regulator of energy metabolism, and time-restricted feeding has been proven to directly improve energy metabolism in mouse iWAT[27], therefore, we chose iWAT for subsequent study. We isolated and purified iWAT mitochondria and detected the mitochondrial markers TOM20 and OPA1, which are expressed only in mitochondria (online Supplementary Fig. S1C). Through Janus Green B staining, we observed a reduction in the number of mitochondria in the IF group of mice (online Supplementary Fig. S1D). Next, the changes in mitochondrial morphology were explored. We observed mouse iWAT under a TEM. The mitochondrial morphology of iWAT after IF tended to be prolonged, showing

a mitochondrial fusion morphology (Fig. 1(d)). Interestingly, we also observed that the HFD caused mitochondrial division (Fig. 1(d)). Meanwhile, IF significantly increased the mitochondrial AR ($P < 0.01$) (Fig. 1(e)). In addition, IF significantly increased the expression of the mitochondrial fusion protein OPA1 and decreased the expression of the fission proteins FIS1 and MFF ($P < 0.01$) (Fig. 1(f)). IF also significantly increased the mRNA levels of mitochondrial the fusion genes Opa1 and Mfn2 ($P < 0.01$) and decreased the mRNA levels of the mitochondrial division genes Fis1 and Drp1 ($P < 0.05$) (Fig. 1(g)). Therefore, the above results indicate that IF promotes iWAT mitochondrial fusion in HFD mice.

Intermittent fasting partially promotes mitochondrial fusion in wild-type and obese mice

Meanwhile, we administered IF procedures on C57BL/6 WT and leptin-deficient obese mice (ob/ob) mice, aiming to explore whether IF has an effect on the morphology and number of mitochondria in both types of mice. In WT mice, after isolating iWAT mitochondria and staining them with Janus Green B, the number of iWAT mitochondria in WT mice was also reduced (online Supplementary Fig. S2A). Observations under TEM showed that the mitochondrial morphology after IF tended to be extended, and it also had an increased mitochondrial AR, showing a mitochondrial fusion morphology (Fig. 2(a)). IF significantly increased the expression of the mitochondrial fusion protein OPA1 ($P < 0.05$); however, the expression of the fission proteins FIS1 ($P = 0.83$) and MFF ($P = 0.61$) was not significantly different (Fig. 2(b)). In addition, IF significantly increased the mRNA level of the mitochondrial fusion gene Opa1 ($P < 0.05$) and reduced the mRNA levels of the mitochondrial division gene Fis1 ($P < 0.01$) (Fig. 2(c)). The results indicate that IF promotes iWAT mitochondrial fusion in WT mice. In ob/ob mice, we found that IF also reduced the number of iWAT mitochondria (online Supplementary Fig. S2B). However, IF showed no significant change in the mitochondrial AR in ob/ob mice ($P = 0.49$) (Fig. 2(d)). Although IF significantly increased the expression of the mitochondrial fusion protein OPA1 ($P < 0.01$), the expression of FIS1 ($P = 0.16$) and MFF ($P = 0.25$) was not significantly different (Fig. 2(e)). Meanwhile, IF significantly reduced the mRNA level of the mitochondrial division gene Fis1 ($P < 0.05$), but there were no significant changes in the other mitochondrial fusion- and division-related genes Opa1 ($P = 0.052$), Mfn2 ($P = 0.061$) and Drp1 ($P = 0.21$) (Fig. 2(f)). Thus, the above results indicate that IF partially promotes iWAT mitochondrial fusion in WT or ob/ob mice but is much less significant than IF in HFD mice, especially genetically obese ob/ob mice.

Intermittent fasting improves mitochondrial function in mouse inguinal white adipose tissue

Mitochondrial fusion is usually accompanied by an improvement in mitochondrial function[28]. Therefore, we explored whether IF affects the mitochondrial function in HFD, WT or ob/ob mice. We used a JC-1 fluorescent probe to detect the mitochondrial membrane potential of mouse iWAT. In HFD mice, JC-1 staining showed increased red fluorescence, and the ratio of red to green fluorescence also increased significantly

($P < 0.01$); that is, the mitochondrial membrane potential increased (online Supplementary Fig. S3A). Next, the ATP content of mouse iWAT was detected, and results showed that IF significantly promoted ATP production ($P < 0.01$) (Fig. 3(a)). Subsequently, RT-qPCR was applied to detect the mtDNA copy number in mouse iWAT. The results in Fig. 3(b) demonstrated that IF significantly increased the copy number of mitochondrial DNA ($P < 0.01$). Following the detection of the mRNA expression of mitochondrial function-related genes under IF, the results showed that IF significantly increased the mRNA expression levels of Tfam, Uqcrc, ATP5a1, Cox4i1 and Sdhb (Fig. 3(c)). All of the above results indicate that IF has a significant impact on improving the mitochondrial function of HFD mice. In WT mice, after IF, the mitochondrial membrane potential was significantly increased (online Supplementary Fig. S3B). IF also promoted the production of ATP ($P < 0.01$) (Fig. 3(d)), but the effects on the mtDNA copy number were not significant ($P = 0.065$) (Fig. 3(e)). Moreover, the mRNA expression of the mitochondrial function-related genes Tfam, Uqcrc, ATP5a1 and Sdhb was significantly increased (Fig. 3(f)). Interestingly, similar results with WT mice were obtained from ob/ob mice after IF. Manifesting as a significant increase in mitochondrial membrane potential (online Supplementary Fig. S3C) and ATP production (Fig. 3(g)), the mtDNA copy number exhibited an upwards trend ($P = 0.074$) (Fig. 3(h)). However, the mitochondrial function-related genes showed no significant changes and even showed significant downregulation of ATP5a1 and Cox4i1 (Fig. 3(i)). Overall, our results indicate that the effect of IF on mitochondrial fusion and function was most remarkable in diet-induced obese (HFD) mice, and there was a tendency to promote mitochondrial function in WT mice and ob/ob mice, but the tendency was not as significant as that in HFD mice.

Intermittent fasting induces SIRT3 expression and protein deacetylation in inguinal white adipose tissue of high-fat diet mice

To elucidate the proteomic changes induced by IF in HFD mice to explain the molecular mechanisms by which IF improves mouse health, we performed a label-free proteomic analysis of HFD mouse iWAT. Meanwhile, we extracted the total protein of iWAT from HFD mice and detected its acetylation level. The results showed that IF significantly promoted the deacetylation of iWAT protein in HFD mice ($P < 0.05$) (Fig. 4(a)). Subcellular structural localisation analysis revealed that 22 % of proteins with altered acetylation levels were localised to mitochondria (Fig. 4(b)). The cluster analysis heatmap based on GO enrichment shows that IF activates NAD (Fig. 4(c)), which has a positive effect on mouse iWAT. In addition, the NAD+ content was also consistent with the sequencing results, and IF significantly increased the NAD+ content of mouse iWAT ($P < 0.01$) (Fig. 4(d)), which also indicated inhibition of the acetylation level. The above results illustrate that IF promotes the deacetylation of iWAT protein in HFD mice. Several studies have demonstrated that Sirt3 is activated during IF and shows higher deacetylation of mitochondrial proteins in response to mitochondrial metabolism and obesity progression[29,30]. Therefore,
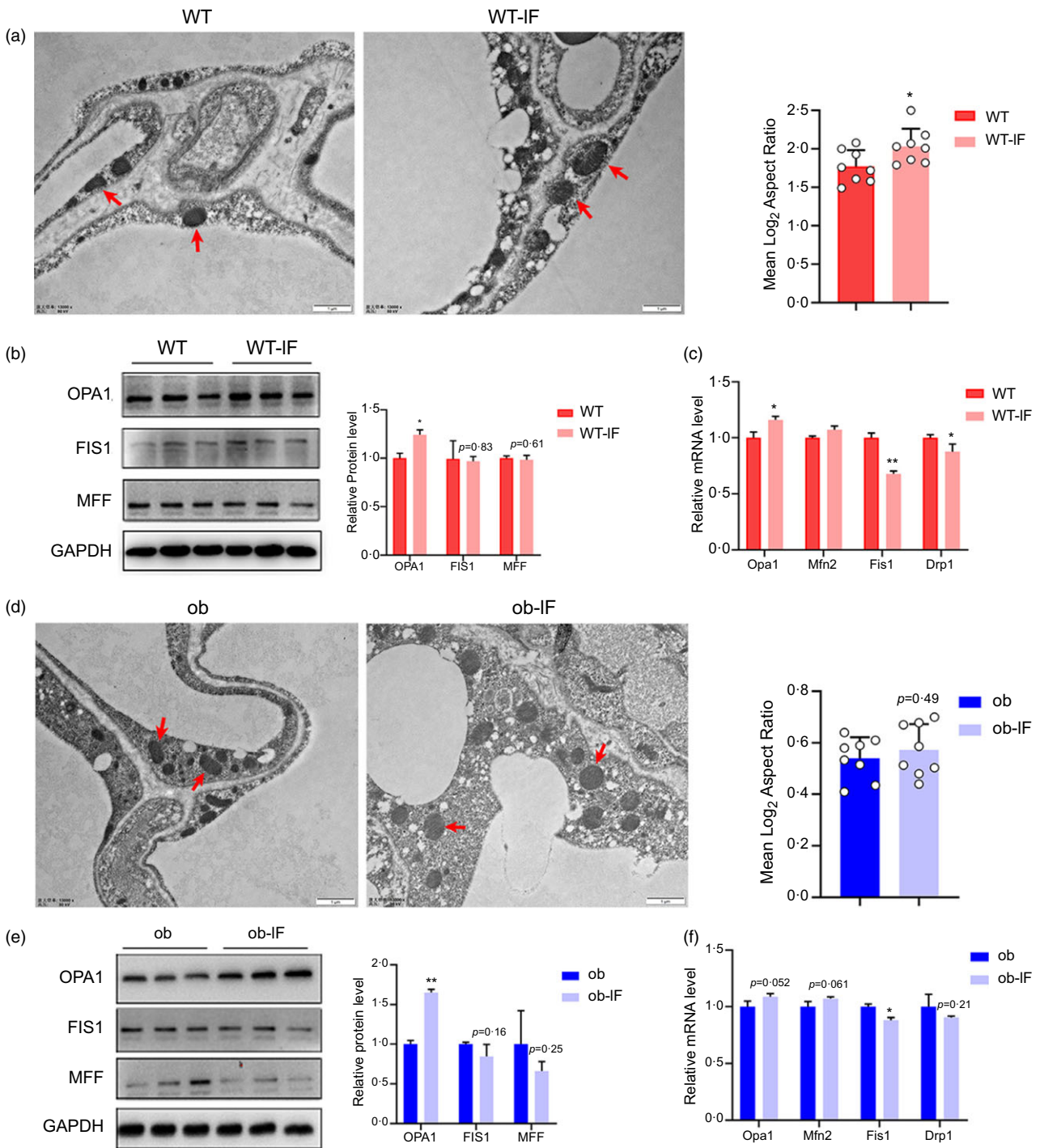
Fig. 2. IF leads to a tendency for mitochondria to fuse in wild-type and obese mice. (a) TEM image of WT (Left) and WT-IF (Right) mouse iWAT, arrows point to mitochondria. Scale bar, 1 μm. And mitochondrial aspect ratio quantification, $n\,8$. (b) Western blotting of mitochondrial fusion and division-related protein and its quantification, $n\,3$. (c) RT-qPCR of mitochondrial fusion and division-related gene, $n\,4$. (d) TEM image of WT (Left) and WT-IF (Right) mouse iWAT, arrows point to mitochondria. Scale bar, 1 μm. And mitochondrial aspect ratio quantification, $n\,8$ each group. (e) Western blotting of mitochondrial fusion and division-related protein and its quantification, $n\,3$. (f) RT-qPCR of mitochondrial fusion and division-related gene, $n\,4$. $*P < 0.05$, $**P < 0.01$ compared with control group. Data are mean ± SEM. IF, intermittent fasting; WT, wild type; TEM, transmission electron microscopy

the effect of IF on Sirtuin expression in the iWAT of HFD mice was further explored. IF significantly increased the mRNA expression level of Sirt3 ($P < 0.05$); however, there was no significant effect on Sirt1 ($P = 0.075$), Sirt2 ($P = 0.37$) or Sirt5 ($P = 0.56$) (Fig. 4(e)). IF also increased the protein expression

of SIRT3 ($P < 0.05$) (Fig. 4(f)). The enrichment analysis of the KEGG pathway shows that the protein modification level of the TCA cycle metabolism pathway changed significantly (Fig. 4(g)). The heatmap of the proteins corresponding to the differentially modified sites shows that MDH2 is the key enzyme
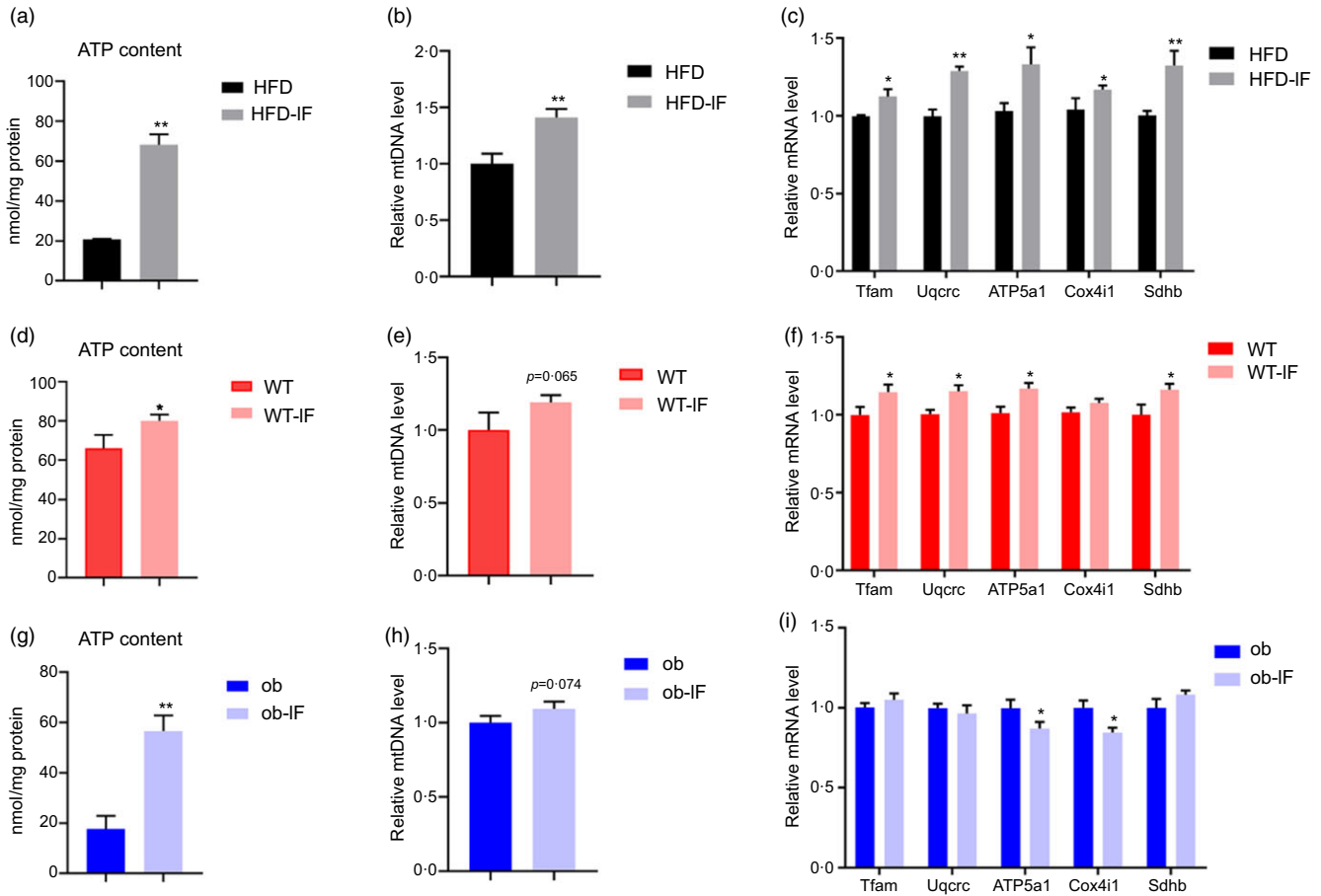
Fig. 3. IF improves mitochondrial function of mice iWAT. (a, d and g) Measurement of mitochondrial ATP content in mouse iWAT, n 3. (b, e and h) Measurement of mtDNA in mouse iWAT, n 4. (c, f and i) RT-qPCR of mitochondrial function-related genes in mouse iWAT, n 4. $*P < 0.05$, $**P < 0.01$ compared with control group. Data are mean ± SEM. IF, intermittent fasting.

of the TCA cycle in the most significantly different modifiable proteins (Fig. 4(h)). The cluster analysis heatmap based on GO enrichment shows that the biological process of mitochondrial membrane composition changed significantly (Fig. 4(i)), indicating that protein deacetylation caused by IF is closely related to the changes in mitochondrial membrane components. Overall, our results indicate that IF deacetylates mitochondrial proteins by promoting Sirt3 expression in iWAT of HFD mice. Sirt3-mediated protein deacetylation may be an important process in the regulation of energy metabolism by IF.

Sirt3 promotes mitochondrial fusion and improves mitochondrial function

IF regulates mitochondrial fusion and fission dynamics, and Sirt3 is closely related to metabolic improvements caused by IF. However, the mechanism of Sirt3-induced deacetylation levels of mitochondrial metabolism-related proteins and mitochondrial fusion and fission dynamics is still unknown. Thus, we further explored whether Sirt3 regulates mitochondrial dynamics or improves mitochondrial function. The Sirt3 overexpression vector was constructed using the pc-DNA3·1 plasmid. After treating the adipocytes with pc-Sirt3 and si-Sirt3, the overexpression and interference efficiency of pc-Sirt3 and si-Sirt3 were

significant ($P < 0.05$) (Fig. 5(a)). Next, we isolated and purified adipocyte mitochondria after treatment with pc-Sirt3 and si-Sirt3 (online Supplementary Fig. S4A). Using Janus Green B staining and the mitochondrial probe mitoTracker, which labels mitochondria in cells, we demonstrated that pc-Sirt3 reduces the number of adipocyte mitochondria (Fig. 5(b) and online Supplementary S4B). More importantly, pc-Sirt3 increased the mRNA levels of Opa1 and Mfn2 and inhibited Drp1 and Fis1 ($P < 0.05$) (Fig. 5(c)). At the protein expression level, pc-Sirt3 increased the expression level of the fusion protein OPA1 ($P < 0.01$) and inhibited the fission proteins FIS1 and MFF ($P < 0.05$) (Fig. 5(d)). The above results indicate that Sirt3 promotes the mitochondrial fusion of adipocytes. We further explored the effect of Sirt3 on mitochondrial function. The ATP content of adipocytes increased after pc-Sirt3 treatment ($P < 0.05$), as si-Sirt3 inhibited ATP production ($P < 0.05$) (Fig. 5(e)). In addition, pc-Sirt3 increased adipocyte mtDNA ($P < 0.05$) (Fig. 5(f)). pc-Sirt3 increased the mRNA expression of the mitochondrial function markers ATP5a1, Sdhb, Tfam and Ndufb8 ($P < 0.05$) (Fig. 5(g)). Dysregulation of adipose tissue energy homeostasis is often accompanied by increased ROS levels[31]. By measuring ROS production, we found that pc-Sirt3 inhibited adipocyte ROS production, while si-Sirt3 produced the opposite result ($P < 0.05$) (online
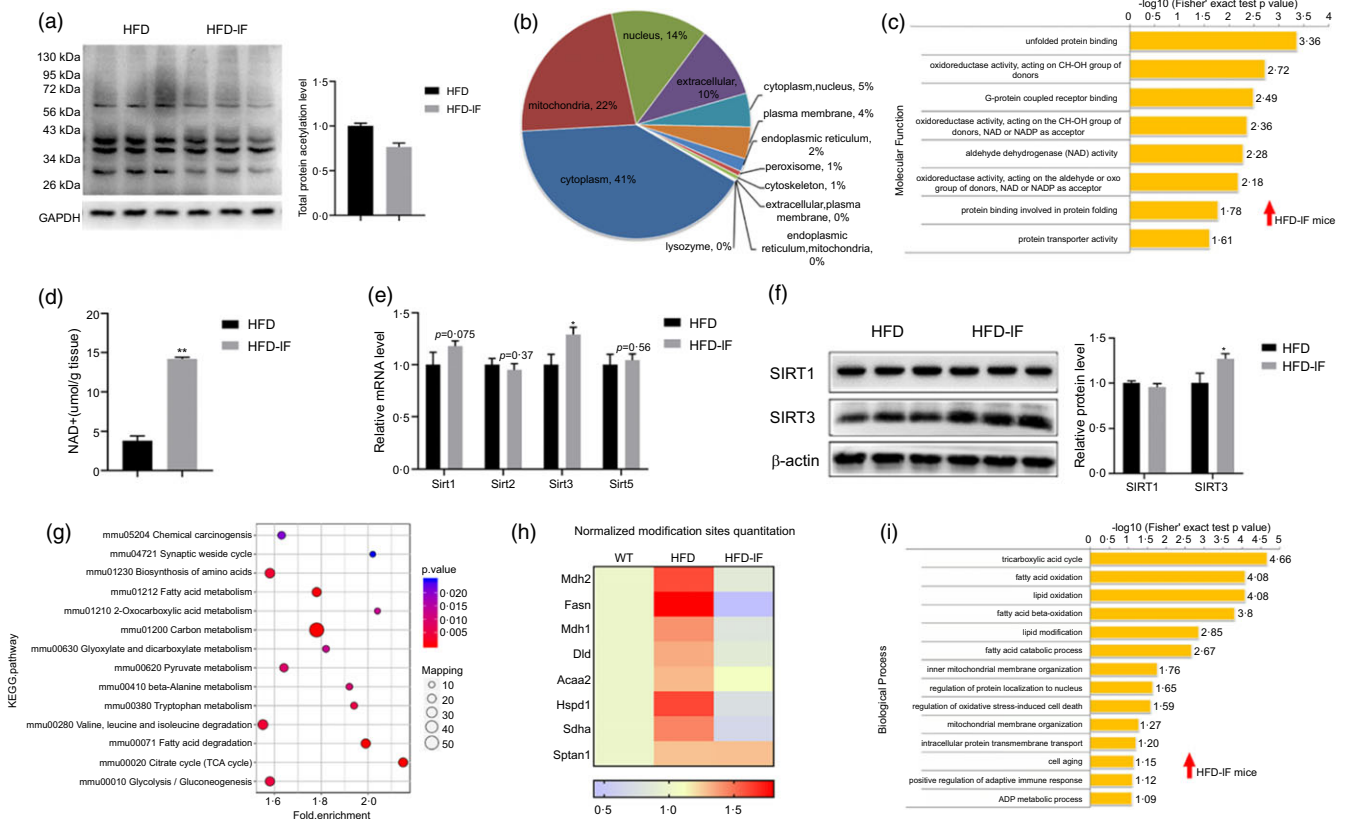
Fig. 4. IF induces Sirt3 expression and protein deacetylation in iWAT of HFD mice. (a) Protein acetylation level in HFD (Left) and HFD–IF (Right) mouse iWAT and its quantification, n 3 each group. (b) Subcellular structural localisation of proteins corresponding to differentially expressed acetylation sites in HFD–IF group compared with HFD group. (c) Cluster analysis of upregulated molecular function in HFD–IF group based on GO enrichment. (d) Measurement of NAD+ content between HFD with HFD–IF mouse iWAT, n 4 each group. (e) mRNA expression of sirtuins family genes, n 4 each group. (f) protein expression of sirtuins family genes and quantification, n 3 each group. (g) KEGG pathway enrichment of proteins corresponding to differentially modified sites in HFD–IF group compared with HFD group. (h) Differentially modified sites analysis in HFD–IF group compared with HFD group. (i) Cluster analysis of upregulated biological process in HFD–IF group based on GO enrichment. *$P < 0.05$, **$P < 0.01$ compared with control group. Data are mean ± SEM. HFD, high-fat diet; IF, intermittent fasting.

Supplementary Fig. S4C). The above results indicate that Sirt3 improves mitochondrial function by promoting mitochondrial fusion in adipocytes.

Sirt3 deacetylates Mdh2 and promotes mitochondrial fusion by inhibiting the JNK-FIS1 pathway

According to the sequencing results, the protein modification level of the metabolic pathway of the TCA cycle changes significantly, and Mdh2, the most significant modifiable protein is the key enzyme of the TCA cycle (Fig. 4(g) and (h)). Sirt3 is known as an NAD+-dependent deacetylase[19]. To verify this result, the NAD+ content of adipocytes treated with pc-Sirt3 and si-Sirt3 was first detected, Fig. 6(a) shows that pc-Sirt3 increased the NAD+ content in adipocytes ($P < 0.05$), and si-Sirt3 reduced the NAD+ content ($P < 0.05$). Furthermore, the total protein acetylation level of adipocytes was tested, and pc-Sirt3 inhibited the acetylation level ($P < 0.01$), while si-Sirt3 showed the opposite effect (Fig. 6(b)). To explore whether Sirt3 induced by IF modulates Mdh2 acetylation levels, the Mdh2 protein of adipocytes treated with pc-Sirt3 and si-Sirt3 was purified by IP, and its acetylation level was detected. The result showed that pc-Sirt3 deacetylated Mdh2 ($P < 0.01$) (Fig. 6(c)). The JNK-FIS1 pathway may play an important role in the regulation of mitochondrial

fusion and fission and mitochondrial function[32]. Therefore, the JNK inhibitor SP600125 (SP) and JNK activator anisomycin (Ani) were used to treat adipocytes. As shown in Fig. 6(d), pc-Sirt3 inhibited the protein levels of p-JNK/JNK and FIS1 ($P < 0.05$). After applying the inhibitor SP, the inhibitory effect of pc-Sirt3 on p-JNK/JNK and FIS1 was more significant ($P < 0.05$), and this inhibitory effect was weakened after supplementing the agonist Ani (Fig. 6(d)). The above results indicate that Sirt3 deacetylates Mdh2 and regulates the JNK-FIS1 pathway. To explore whether Sirt3 affects the JNK-FIS1 pathway by regulating the level of Mdh2 acetylation, we treated adipocytes with Cas9-Mdh2 and knocked out Mdh2 (Fig. 6(e)) and then treated Mdh2$^{-/-}$ adipocytes with pc-Sirt3 or si-Sirt3 to detect the protein expression levels of p-JNK, JNK and FIS1. As shown in Fig. 6(f), pc-Sirt3 inhibited the expression of p-JNK and FIS1 ($P < 0.01$), but the inhibitory effect of pc-Sirt3 on the JNK-FIS1 pathway was significantly reduced after Mdh2 was knocked out ($P < 0.05$). In addition, pc-Sirt3 promoted the mRNA levels of the mitochondrial fusion genes Opa1 and Mfn2 ($P < 0.05$) and strongly inhibited the expression of Fis1 ($P < 0.01$). However, when Mdh2 was knocked down, this trend was weakened after knocking down Mdh2 (Fig. 6(g)). Overall, our results reveal that Sirt3 inhibits the JNK-FIS1 pathway by deacetylating Mdh2 to promote mitochondrial fusion.
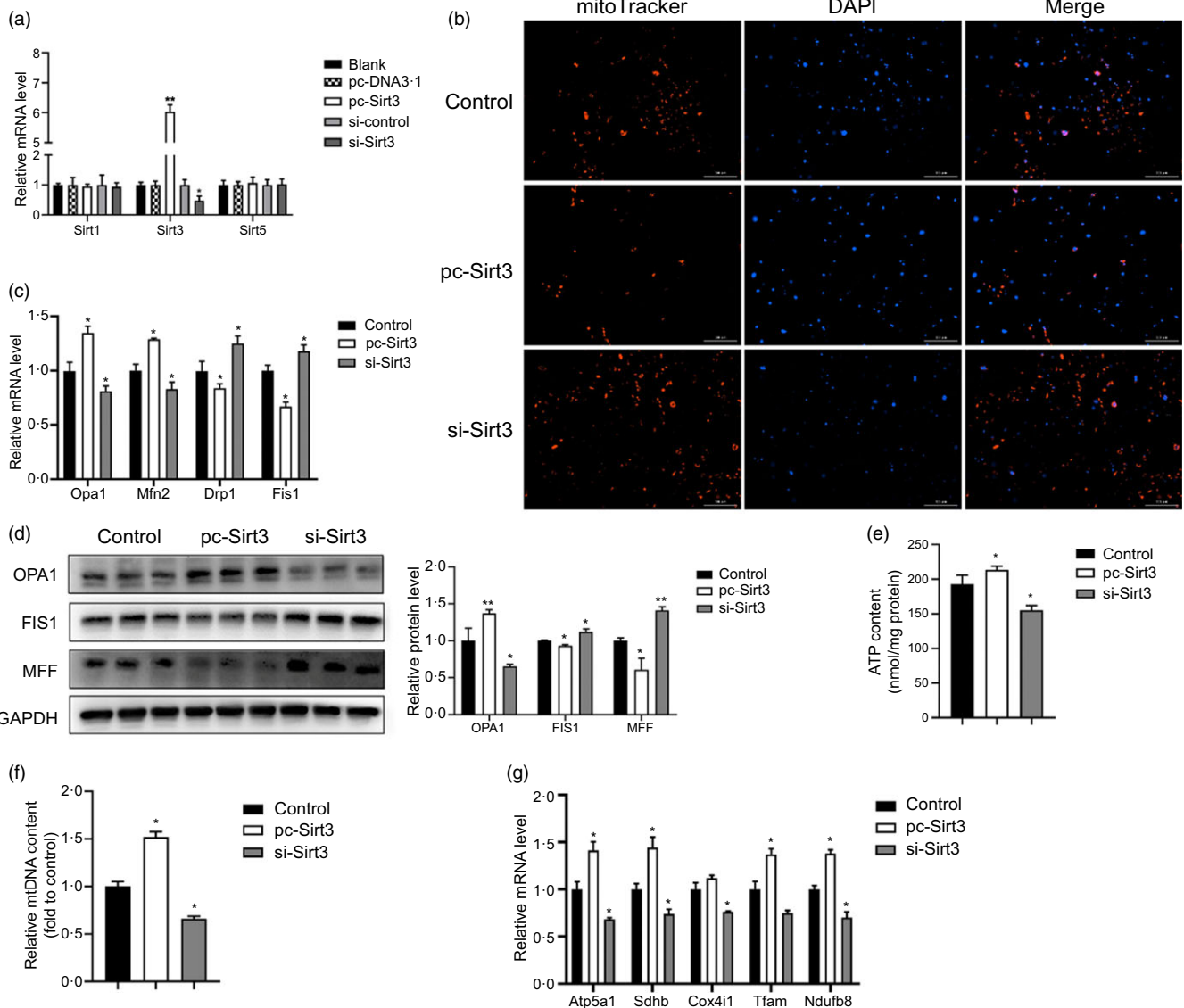
Fig. 5. Sirt3 promotes mitochondrial fusion and improves mitochondrial function. (a) Overexpression and interference efficiency of pc-Sirt3 and si-Sirt3, *n* 4. (b) mitoTracker probe staining. Scale bar, 300 μm. (c) RT-qPCR of mitochondrial fusion and division-related gene, *n* 4. (d) Western blotting of mitochondrial fusion and division-related protein and its quantification, *n* 3. (e) Measurement of adipocyte mitochondrial ATP content, *n* 3. (f) Measurement of adipocyte mtDNA, *n* 4. (g) RT-qPCR of adipocyte mitochondrial function-related gene, *n* 4. $^*P < 0.05$, $^{**}P < 0.01$ compared with control group. Data are mean ± SEM.

Discussion

IF has drawn increasing attention in recent years and is considered a novel and promising method for weight loss and inflammation reduction. In addition, IF is believed to have great potential in improving long-term health. Studies have shown that IF can reduce weight and have an effect on heart protection[33,34]. This protective effect may be related to decreased lipid deposition, increased adiponectin concentration and decreased leptin and LDL concentrations[35]. During fasting, fat is consumed after the activation of the gluconeogenesis process, and then the body supplies energy by glucose-ketone (G-to-K) conversion[36,37]. Therefore, IF is effective for reducing lipid deposition, as well as inducing a series of biochemical changes to improve their resistance to stress, injury and disease[36,38]. In our study,

IF significantly reduced body weight in HFD mice, demonstrating the health benefits of IF in obese patients.

Mitochondria participate in core central metabolic pathways, particularly adipose tissue-related energy metabolism processes[39]. According to TEM observations from previous studies, the skeletal muscle mitochondria of subjects with type 2 diabetes and obesity are smaller than those of fasted and lean volunteers, and the bioenergetic function of their mitochondria is impaired[40]. In our study, three models, diet-induced obese mice (HFD mice), normal mice (WT mice) and genetically obese mice (ob/ob mice), were subjected to TEM to investigate the effects of IF on the morphology of mitochondria in adipose tissue. As expected, IF significantly increased the mitochondrial AR in HFD mice and promoted mitochondrial fusion, while the fusion of the other two models only slightly increased. Previous
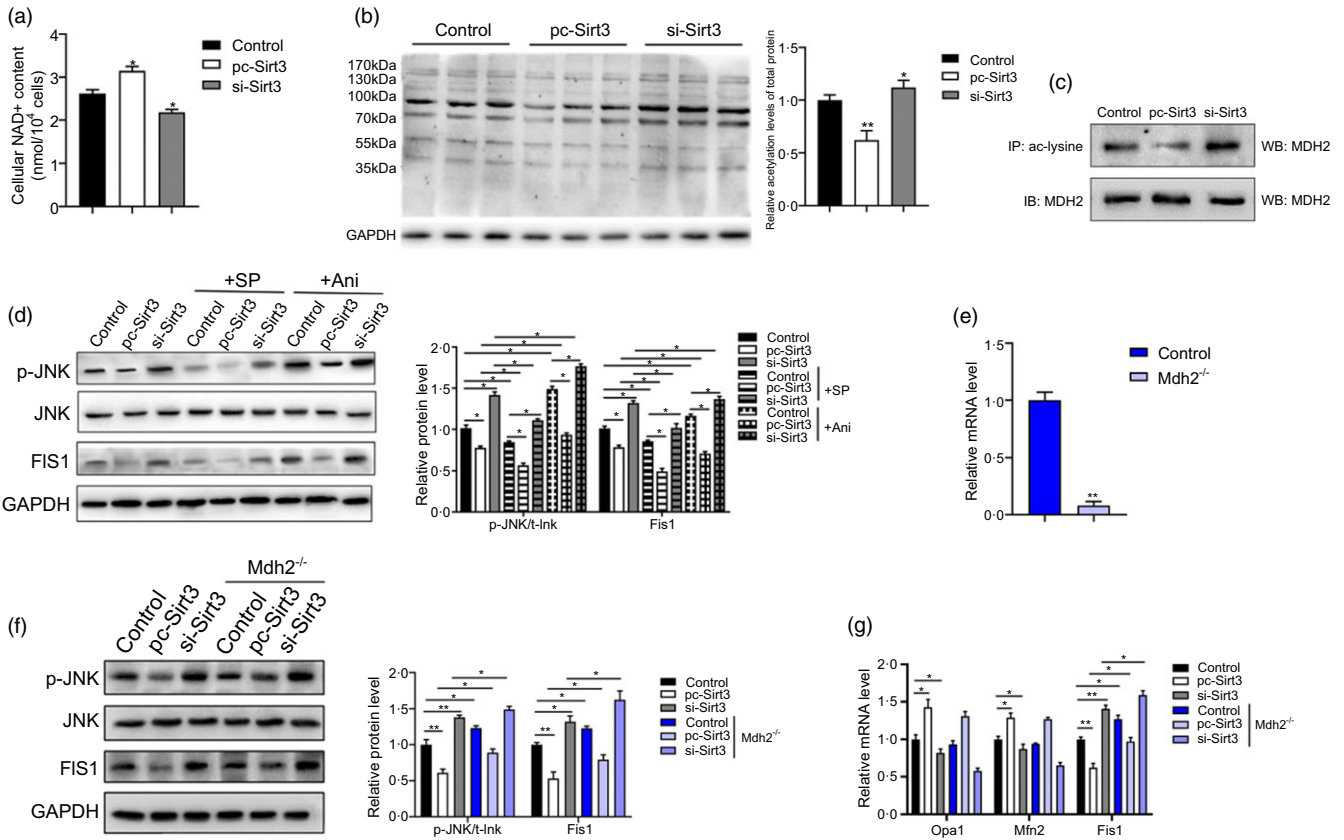
Fig. 6. Sirt3 deacetylates Mdh2 and promotes mitochondrial fusion by inhibiting the JNK-FIS1 pathway. (a) Measurement of adipocyte NAD+ content, *n* 3. (b) Adipocyte total protein acetylation level and its quantification, *n* 3. (c) Co-immunoprecipitation of Mdh2 acetylation level and its quantification. (d) P-JNK, JNK and FIS1 protein levels and their quantification after SP or Ani treatment and protein quantitative, *n* 3. (e) Mdh2 mRNA levels in adipocytes treated with 2300-Cas9 + Target 1 and 2300-Cas9 + Target 2, *n* 4. (f) P-JNK, JNK and FIS1 protein levels and their quantification, *n* 3. (g) RT-qPCR of mitochondrial fusion and division-related genes, *n* 4. *$P < 0.05$, **$P < 0.01$ compared with control group. Data are mean ± SEM.

studies have performed IF on ob/ob mice and did not demonstrate significant weight gain or fat loss, while they showed higher glucose tolerance and postprandial insulin[41], indicating that IF may not be an effective way to improve metabolism in ob/ob mice, which is also consistent with our research. In addition, IF significantly upregulated the mitochondrial fusion genes Opa1 and Mfn2 and downregulated the fission genes Fis1 and Drp1. At the protein level, the fusion protein OPA1 is significantly upregulated, while the fission proteins FIS1 and MFF are downregulated. These results suggest that IF significantly improves mitochondrial morphology in HFD mice.

Adipose tissue is a key regulator of energy metabolism, time-restricted feeding directly improves energy metabolism in mouse iWAT[27], and alterations in energy metabolism are accompanied by changes in mitochondrial morphology and function[42,43]. In obese mice, mitochondrial dysfunction and decreased ATP production as well as a reduction in the necessary metabolic cofactor NAD+ were found[44]. Therefore, maintaining mitochondrial function is vital to mammals. However, there are few discussions on the mitochondrial function of adipose tissue with IF. We further explored the alteration of mitochondrial function and iWAT energy metabolism in three models after IF. In HFD mice, IF significantly improved the membrane potential and increased ATP synthesis and mtDNA copy number. More importantly, IF upregulated the expression of mitochondrial

function-related genes in HFD mice, including mitochondrial transcription factor A (TFAM), which regulates mtDNA replication and transcription, a marker of the mitochondrial oxidative phosphorylation complex, Ubiquinol-cytochrome c reductase core protein (Uqcrc), ATP synthase *α*-subunit (Atp5a1), cytochrome c oxidase subunit 4 isoform 1 (Cox4i1) and succinate dehydrogenase subunit B (Sdhb). IF improved mitochondrial function, and interestingly, this phenomenon was most obvious in HFD mice, which provides evidence for our further study on HFD mice. In addition, we measured serum concentrations of the major metabolites in mice. After IF, serum LDL, TC and TG levels were decreased, and HDL levels were increased. Moreover, we found that IF improved glucose tolerance in HFD mice by glucose tolerance test and insulin tolerance test, which is consistent with other studies to date[45]. It is noted that HDL concentrations differed depending on the time of fasting, inactive (light) or active (dark), and HDL levels appeared to be lower when fasting during active periods[46]. Moreover, it has even been shown that inappropriate fasting times directly modulate the energy homeostasis of adipose tissue[27]. This suggests that the duration of fasting directly links to the degree of metabolic improvement and that the fasting program is critical to improving metabolism. However, HDL is higher during both inactive and active periods compared with *ad libitum*, and IF also improves HFD-induced obesity, which is also consistent

with our findings. In conclusion, our study proves that IF enhances mitochondrial function and improves the metabolic health of HFD mice.

Sirtuins are NAD(+)-dependent protein deacetylases that function in response to stress[19], which includes calorie restriction (IF) and other metabolic stresses. For example, IF activates SIRT1 expression in diabetic model mice (ob/ob) and alleviates diabetes-induced visual impairment and inflammatory responses in the bone marrow[47], and Sirt3 mediates IF to reduce neuroinflammation[48], SIRT3 regulates mitochondrial metabolism and fatty acid oxidation in brown adipose tissue and the liver through deacetylation of mitochondria-associated proteins[49]. In our research, we found that IF is associated with an increase in protein deacetylation levels of HFD mice. Due to the effect of Sirt3 on regulating mitochondrial protein acetylation and the remarkable performance of IF in activating high expression of Sirt3, we speculate that Sirt3 regulates the acetylation of mitochondrial-related proteins during IF. The GO enrichment shows that the activity of NAD+ is increased, and IF significantly elevated SIRT3 protein expression without altering SIRT1 expression. Moreover, we found that the biological process of mitochondrial membrane composition varied significantly during IF. Therefore, we further explored the mechanism of SIRT3 action during IF.

Sirt3 is located in the mitochondrial matrix and is a member of the sirtuin family that relies on NAD+ for deacetylation[50]. Sirt3 is a deacetylase that regulates the acetylation of most lysines inside mitochondria and mitochondrial function[51–53]. Overexpression of Sirt3 alleviated mitochondrial disorders by enhancing mitochondrial fusion triggered by OPA1[54] and reduces mitochondrial damage, thereby maintaining mitochondrial morphology and protecting mitochondrial function[55]. The increase in Sirt3 protein may increase mitochondrial fusion signals, improve mitochondrial morphology and reduce oxidative stress[56]. However, the effect of Sirt3 on mitochondrial fusion and mitochondrial function of adipocytes is still unclear. Thus, we constructed SIRT3 overexpression and interference vectors to confirm the mechanism by which Sirt3 improves adipocyte metabolism. As expected, Sirt3 overexpression significantly promoted mitochondrial fusion and improved mitochondrial function in adipocytes, whereas Sirt3 knockdown had the opposite inhibitory effect.

Meanwhile, according to our heatmap of the corresponding protein at the differentially modified sites, MDH2 is a key enzyme in the TCA cycle that provides a target for elucidating the deacetylation effect of Sirt3 on mitochondrial metabolism-related proteins. Rardin *et al.*[57] used a rigorous label-free quantitative MS method to analyse changes in lysine acetylation in mouse liver mitochondria without Sirt3, and sequencing indicated that Sirt3 regulates protein acetylation in a variety of metabolic pathways. In addition, Sirt3 could directly change the acetylation level of MDH2. MDH are a group of NAD-dependent dehydrogenases that catalyse the conversion of substrates between NAD and NADH[58]. This process is an important step in the mitochondrial TCA cycle. Recent research has identified that the acetylation level of Mdh2 is significantly increased during adipogenesis[59]. These studies indicate that the acetylation level of Mdh2 is affected by the energy state of cells. Here, we demonstrate that Sirt3 significantly inhibits the level of cellular acetylation. Through sequencing, we screened MDH2 as a target for deacetylation by SIRT3, and in combination with IP experiments, we demonstrated that Sirt3 directly deacetylates MDH2. Hence, SIRT3 is able to directly communicate and alter the acetylation level of MDH2[60,61]. Our research confirms this conclusion.

Previous studies have demonstrated that specific knockdown of Sirt3 upregulates the expression of the JNK pathway[62] and that Sirt3 upregulation reduces endoplasmic reticulum stress and blocks the proapoptotic JNK pathway[63]. Here, our experiments with adipocytes treated with the JNK inhibitor SP or activator Ani highlight and confirm this direct link between Sirt3 and the JNK pathway. Sirt3 amplifies the inhibitory effect of SP and attenuates the activation effect of Ani. In addition, studies have demonstrated that the JNK-FIS1 pathway is associated with improved mitochondrial dysfunction[64,65]. However, whether Sirt3 connects to MDH2 to communicate with the JNK-FIS1 pathway has not been investigated. Thus, we constructed a CAS9-Mdh2 vector to knock down Mdh2 and then overexpressed or interfered with Sirt3, and the results showed that the inhibition of p-JNK and FIS1 by SIRT3 was significantly reduced after MDH2 knockdown. Suggesting that Sirt3 inhibition of the JNK-FIS1 pathway is achieved through deacetylation of MDH2, our study provides a more in-depth theoretical study of Sirt3 regulation of mitochondrial fusion division kinetics.

In general, our research reveals a regulatory mechanism by which energy restriction controls mitochondrial energy homeostasis through animal adipocyte protein acetylation levels. In addition, this research provides theoretical support for the study of energy limitation and animal energy metabolism.

Limitations of study

There are still some limitations to our current study. Our results show that IF improves mitochondrial fusion and mitochondrial function in WT mice fed a normal diet and in ob/ob mice, although the effects are not as pronounced as in HFD mice. Further research may focus on different animal models. In addition, the inhibitory effect of Sirt3 on the JNK-FIS1 pathway was only weakened after MDH2 knockdown, but did not completely disappear, suggesting that the pathway through which Sirt3 regulates mitochondrial fusion dynamics is a much more complex process and still needs to be studied in more depth.

Acknowledgements

Supplementary material

For supplementary material/s referred to in this article, please visit https://doi.org/10.1017/S000711452300048X

References

1. Bhargava P & Schnellmann R (2017) Mitochondrial energetics in the kidney. *Nat Rev Nephrol* **13**, 629–646.
2. Mansouri A, Gattolliat C & Asselah T (2018) Mitochondrial dysfunction and signaling in chronic liver diseases. *Gastroenterology* **155**, 629–647.
3. Li Q, Gao Z, Chen Y, *et al.* (2017) The role of mitochondria in osteogenic, adipogenic and chondrogenic differentiation of mesenchymal stem cells. *Protein Cell* **8**, 439–445.
4. Von Stockum S, Nardin A, Schrepfer E, *et al.* (2016) Mitochondrial dynamics and mitophagy in Parkinson's disease: a fly point of view. *Neurobiol Dis* **90**, 58–67.
5. Chaudhari SN & Kipreos ET (2017) Increased mitochondrial fusion allows the survival of older animals in diverse C. elegans longevity pathways. *Nat Commun* **8**, 182.
6. Losón OC, Song Z, Chen H, *et al.* (2013) Fis1, Mff, MiD49, and MiD51 mediate Drp1 recruitment in mitochondrial fission. *Mol Biol Cell* **24**, 659–667.
7. Dalmasso G, Marin Zapata PA, Brady NR, *et al.* (2017) Agent-based modeling of mitochondria links sub-cellular dynamics to cellular homeostasis and heterogeneity. *PLoS ONE* **12**, e0168198.
8. Liesa M & Shirihai OS (2013) Mitochondrial dynamics in the regulation of nutrient utilization and energy expenditure. *Cell Metab* **17**, 491–506.
9. Rynders CA, Thomas EA, Zaman A, *et al.* (2019) Effectiveness of intermittent fasting and time-restricted feeding compared to continuous energy restriction for weight loss. *Nutrients* **11**, 2442.
10. Baumeier C, Kaiser D, Heeren J, *et al.* (2015) Caloric restriction and intermittent fasting alter hepatic lipid droplet proteome and diacylglycerol species and prevent diabetes in NZO mice. *BBA* **1851**, 566–576.
11. Yang W, Cao M, Mao X, *et al.* (2016) Alternate-day fasting protects the livers of mice against high-fat diet-induced inflammation associated with the suppression of Toll-like receptor 4/nuclear factor κB signaling. *Nutr Res* **36**, 586–593.
12. Weir HJ, Yao P, Huynh FK, *et al.* (2017) Dietary restriction and AMPK increase lifespan via mitochondrial network and peroxisome remodeling. *Cell Metab* **26**, 884–896.
13. Liu Y, Cheng A, Li YJ, *et al.* (2019) SIRT3 mediates hippocampal synaptic adaptations to intermittent fasting and ameliorates deficits in APP mutant mice. *Nat Commun* **10**, 1886.
14. Zhang Y, Zhou F, Bai M, *et al.* (2019) The pivotal role of protein acetylation in linking glucose and fatty acid metabolism to β-cell function. *Cell Death Dis* **10**, 66.
15. Shimazu T, Hirschey MD, Hua L, *et al.* (2010) SIRT3 deacetylates mitochondrial 3-hydroxy-3-methylglutaryl CoA synthase 2 and regulates ketone body production. *Cell Metab* **12**, 654–661.
16. De Marchi U, Galindo AN, Thevenet J, *et al.* (2019) Mitochondrial lysine deacetylation promotes energy metabolism and calcium signaling in insulin-secreting cells. *FASEB J* **33**, 4660–4674.
17. Tsuda M, Fukushima A, Matsumoto J, *et al.* (2018) Protein acetylation in skeletal muscle mitochondria is involved in impaired fatty acid oxidation and exercise intolerance in heart failure. *J Cachexia Sarcopenia Muscle* **9**, 844–859.
18. Osborne B, Cooney GJ & Turner N (2014) Are sirtuin deacylase enzymes important modulators of mitochondrial energy metabolism? *BBA* **1840**, 1295–1302.
19. Zhang Y, Wen P, Luo J, *et al.* (2021) Sirtuin 3 regulates mitochondrial protein acetylation and metabolism in tubular epithelial cells during renal fibrosis. *Cell Death Dis* **12**, 847.
20. Samant SA, Zhang HJ, Hong Z, *et al.* (2014) SIRT3 deacetylates and activates OPA1 to regulate mitochondrial dynamics during stress. *Mol Cell Biol* **34**, 807–819.
21. Herr DJ, Baarine M, Aune SE, *et al.* (2018) HDAC1 localizes to the mitochondria of cardiac myocytes and contributes to early cardiac reperfusion injury. *J Mol Cell Cardiol* **114**, 309–319.
22. Herr DJ, Singh T, Dhammu T, *et al.* (2020) Regulation of metabolism by mitochondrial enzyme acetylation in cardiac ischemia-reperfusion injury. *Biochim Biophys Acta Mol Basis Dis* **1866**, 165728.
23. Xiao H, Wang J, Yuan L, *et al.* (2013) Chicoric acid induces apoptosis in 3T3-L1 preadipocytes through ROS-mediated PI3K/Akt and MAPK signaling pathways. *J Agric Food Chem* **61**, 1509–1520.
24. Laursen NB, Kessler R, Fröhli E, *et al.* (1998) Effects of ras transformation on the induction of the IL-1 receptor related T1 gene in response to mitogens, anisomycin, IL-1 and TNFα. *Oncogene* **16**, 575–586.
25. Gómez-Valadés AG, Pozo M, Varela L, *et al.* (2021) Mitochondrial cristae-remodeling protein OPA1 in POMC neurons couples Ca(2+) homeostasis with adipose tissue lipolysis. *Cell Metab* **33**, 1820–1835.
26. Wei D, Li Y, Che M, *et al.* (2022) Melatonin relieves hepatic lipid dysmetabolism caused by aging via modifying the secondary bile acid pattern of gut microbes. *Cell Mol Life Sci* **79**, 527.
27. Hepler C, Weidemann BJ, Waldeck NJ, *et al.* (2022) Time-restricted feeding mitigates obesity through adipocyte thermogenesis. *Science* **378**, 276–284.
28. Chan DC (2020) Mitochondrial dynamics and its involvement in disease. *Annu Rev Pathol* **15**, 235–259.
29. Wang T, Cao Y, Zheng Q, *et al.* (2019) SENP1-Sirt3 signaling controls mitochondrial protein acetylation and metabolism. *Mol Cell* **75**, 823–834.
30. Yang H, Yang T, Baur JA, *et al.* (2007) Nutrient-sensitive mitochondrial NAD+ levels dictate cell survival. *Cell* **130**, 1095–1107.
31. Ahmed B, Sultana R & Greene MW (2021) Adipose tissue and insulin resistance in obese. *Biomed Pharmacother* **137**, 111315.
32. Yao X, Jing X, Guo J, *et al.* (2019) Icariin protects bone marrow mesenchymal stem cells against iron overload induced dysfunction through mitochondrial fusion and fission, PI3K/AKT/mTOR and MAPK pathways. *Front Pharmacol* **10**, 163.
33. Garza-González S, Nieblas B, Solbes-Gochicoa MM, *et al.* (2022) Intermittent fasting as possible treatment for heart failure. *Curr Vasc Pharmacol* **20**, 260–271.
34. Varady KA, Bhutani S, Klempel MC, *et al.* (2013) Alternate day fasting for weight loss in normal weight and overweight subjects: a randomized controlled trial. *Nutr J* **12**, 146.
35. Patterson RE & Sears DD (2017) Metabolic effects of intermittent fasting. *Annu Rev Nutr* **37**, 371–393.
36. Mattson MP, Moehl K, Ghena N, *et al.* (2018) Intermittent metabolic switching, neuroplasticity and brain health. *Nat Rev Neurosci* **19**, 63–80.
37. Wilhelmi de Toledo F, Grundler F, Bergouignan A, *et al.* (2019) Safety, health improvement and well-being during a 4 to 21-d fasting period in an observational study including 1422 subjects. *PLoS ONE* **14**, e0209353.

38. Zhang X, Gao T, Deng S, *et al.* (2021) Fasting induces hepatic lipid accumulation by stimulating peroxisomal dicarboxylic acid oxidation. *J Biol Chem* **296**, 100622.

39. Annesley SJ & Fisher PR (2019) Mitochondria in health and disease. *Cells* **8**, 680.

40. Kelley DE, He J, Menshikova EV, *et al.* (2002) Dysfunction of mitochondria in human skeletal muscle in type 2 diabetes. *Diabetes* **51**, 2944–2950.

41. Kim YH, Lee JH, Yeung JL, *et al.* (2019) Thermogenesis-independent metabolic benefits conferred by isocaloric intermittent fasting in ob/ob mice. *Sci Rep* **9**, 2479.

42. Wu MT, Chou HN & Huang CJ (2014) Dietary fucoxanthin increases metabolic rate and upregulated mRNA expressions of the PGC-1α network, mitochondrial biogenesis and fusion genes in white adipose tissues of mice. *Mar Drugs* **12**, 964–982.

43. Lee JH, Park A, Oh KJ, *et al.* (2019) The role of adipose tissue mitochondria: regulation of mitochondrial function for the treatment of metabolic diseases. *Int J Mol Sci* **20**, 4924.

44. Uddin GM, Youngson NA, Doyle BM, *et al.* (2017) Nicotinamide mononucleotide (NMN) supplementation ameliorates the impact of maternal obesity in mice: comparison with exercise. *Sci Rep* **7**, 15063.

45. Santos HO & Macedo RCO (2018) Impact of intermittent fasting on the lipid profile: assessment associated with diet and weight loss. *Clin Nutr ESPEN* **24**, 14–21.

46. Hanjani N, Zamaninour N, Najibi N, *et al.* (2021) The effects of calorie restriction and time-restricted feeding on IGF1 serum level and lipid profile in male Wister rats with previous obesity. *Int J Prev Med* **12**, 157.

47. Hammer SS, Vieira CP, McFarland D, *et al.* (2021) Fasting and fasting-mimicking treatment activate SIRT1/LXRα and alleviate diabetes-induced systemic and microvascular dysfunction. *Diabetologia* **64**, 1674–1689.

48. Dai S, Wei J, Zhang H, *et al.* (2022) Intermittent fasting reduces neuroinflammation in intracerebral hemorrhage through the Sirt3/Nrf2/HO-1 pathway. *J Neuroinflam* **19**, 122.

49. Hirschey MD, Shimazu T, Goetzman E, *et al.* (2010) SIRT3 regulates mitochondrial fatty-acid oxidation by reversible enzyme deacetylation. *Nature* **464**, 121–125.

50. Schwer B, North BJ, Frye RA, *et al.* (2002) The human silent information regulator (Sir)2 homologue hSIRT3 is a mitochondrial nicotinamide adenine dinucleotide-dependent deacetylase. *J Cell Biol* **158**, 647–657.

51. Peng C, Lu Z, Xie Z, *et al.* (2011) The first identification of lysine malonylation substrates and its regulatory enzyme. *Mol Cell Proteomics* **10**(12), M111.012658.

52. Lombard DB, Alt FW, Cheng HL, *et al.* (2007) Mammalian Sir2 homolog SIRT3 regulates global mitochondrial lysine acetylation. *Mol Cell Biol* **27**, 8807–8814.

53. Sun W, Liu C, Chen Q, *et al.* (2018) SIRT3: a new regulator of cardiovascular diseases. *Oxid Med Cell Longevity* **2018**, 7293861.

54. Wang Q, Xu J, Li X, *et al.* (2019) Sirt3 modulate renal ischemia-reperfusion injury through enhancing mitochondrial fusion and activating the ERK-OPA1 signaling pathway. *J Cell Physiol* **234**, 23495–23506.

55. Wu X, Luo J, Liu H, *et al.* (2020) SIRT3 protects against early brain injury following subarachnoid hemorrhage via promoting mitochondrial fusion in an AMPK dependent manner. *Chin Neurosurg J* **6**, 1.

56. Zhao D, Sun Y, Tan Y, *et al.* (2018) Short-duration swimming exercise after myocardial infarction attenuates cardiac dysfunction and regulates mitochondrial quality control in aged mice. *Oxid Med Cell Longevity* **2018**, 4079041.

57. Rardin MJ, Newman JC, Held JM, *et al.* (2013) Label-free quantitative proteomics of the lysine acetylome in mitochondria identifies substrates of SIRT3 in metabolic pathways. *Proc Natl Acad Sci USA* **110**, 6601–6606.

58. Minárik P, Tomásková N, Kollárová M, *et al.* (2002) Malate dehydrogenases – structure and function. *Gen Physiol Biophys* **21**, 257–265.

59. Kim EY, Han BS, Kim WK, *et al.* (2013) Acceleration of adipogenic differentiation via acetylation of malate dehydrogenase 2. *Biochem Biophys Res Commun* **441**, 77–82.

60. Yang H, Zhou L, Shi Q, *et al.* (2015) SIRT3-dependent GOT2 acetylation status affects the malate-aspartate NADH shuttle activity and pancreatic tumor growth. *EMBO J* **34**, 1110–1125.

61. Guo X, Jiang X, Chen K, *et al.* (2022) The role of palmitoleic acid in regulating hepatic gluconeogenesis through SIRT3 in obese mice. *Nutrients* **14**, 1482.

62. Liang Q, Benavides GA, Vassilopoulos A, *et al.* (2013) Bioenergetic and autophagic control by Sirt3 in response to nutrient deprivation in mouse embryonic fibroblasts. *Biochem J* **454**, 249–257.

63. Yang Y, Gong Z & Wang Z (2019) Yes-associated protein reduces neuroinflammation through upregulation of Sirt3 and inhibition of JNK signaling pathway. *J Recept Signal Transduct Res* **39**, 479–487.

64. Ravi R & Subramaniam Rajesh B (2022) Paraoxonase 2 protects against the CML mediated mitochondrial dysfunction through modulating JNK pathway in human retinal cells. *Biochim Biophys Acta Gen Subj* **1866**, 130043.

65. Naia L, Carmo C, Campesan S, *et al.* (2021) Mitochondrial SIRT3 confers neuroprotection in Huntington's disease by regulation of oxidative challenges and mitochondrial dynamics. *Free Radic Biol Med* **163**, 163–179.